Nanostructued core–shell Sn nanowires @ CNTs with controllable thickness of CNT shells for lithium ion battery

Yu Zhong [a], Xifei Li [a], Yong Zhang [a], Ruying Li [a], Mei Cai [b], Xueliang Sun [a],*

[a] Department of Mechanical and Materials Engineering, University of Western Ontario, London, Ontario N6A 5B9, Canada
[b] General Motors Research and Development Center, Warren, MI 48090-9055, USA

A B S T R A C T

Core–shell structure of Sn nanowires encapsulated in amorphous carbon nanotubes (Sn@CNTs) with controlled thickness of CNT shells was in situ prepared via chemical vapor deposition (CVD) method. The thickness of CNT shells was accurately controlled from 4 to 99 nm by using different growth time, flow rate of hydrocarbon gas (C_2H_4) and synthesis temperature. The microstructure and composition of the coaxial Sn@CNTs were characterized by X-ray diffraction (XRD), scanning electron microscopy (SEM), and high resolution transmission electron microscopy (HRTEM) techniques. Moreover, the Sn@CNTs were studied as anode materials for Li-ion batteries and showed excellent cycle performance. The capacity was affected by the thickness of outer CNT shells: thick CNT shells contributed to a better retention while thin CNT shells led to a higher capacity. The thin CNT shell of 6 nm presented the highest capacity around 630 mAh g^{-1}.

1. Introduction

The lithium ion battery (LIB) has been considered as a very powerful and promising energy source for portable electronic devices due to high energy density [1–5]. However, the commercialized graphite anode only has the low theoretic capacity of 372 mAh g^{-1} [6]. To meet the demands of better performance of LIB, intensive work has been dedicated to find new anode materials which have higher theoretic capacity and better cycling performance, like Sn with theoretic capacity of 994 mAh g^{-1} [7]. However, Sn anode suffers from the big volume change during the charge/discharge process [8], which leads to the pulverization of the anodes and sharply declines the performance of the batteries [9–11]. To solve the problem resulting from the large volume change, nanomaterials as anodes could provide an effective approach for their unique structures and excellent properties [12]. Some significant advantages of nanomaterials as anodes have been revealed: (1) there is void space between the nanostructures which can effectively buffer the volume change during the charge/discharge process; (2) due to the unique structures, they provide quite short diffusion distance for Li ions to insert/extract from the anodes and short path for electron transportation; (3) the nanomaterials possess the huge surface area which could increase the charge/discharge rate [1,13,14].

Some novel nanostructures, like nanopaticles [15], nanowires [16–18], nanotubes [19] and core–shell nanostructures [20–23], have already been employed as anodes in LIBs. Especially in the core–shell structure, the outer layers like carbon as a shell can help to enhance the performance of the batteries [3,12]. Furthermore, more research attentions are paid to one dimensional core–shell nanomaterials consisting of Sn nanomaterials as core and carbon layers as shell. The roles of carbon in the unique core–shell structure have been proposed as: (1) limiting the volume expansion and stabilizing the structure; (2) increasing the electrical conductivity; (3) protecting the nanomaterials from damage in various working environment [3,12,21,24]. These core–shell nanomaterials can be produced via in situ methods. Li et al. [25] reported the in situ synthesis of Sn nanowires encapsulated in amorphous carbon nanotubes. Deng and Lee [26] also presented the fabrication of rambutan-like tin-carbon nanoposites via ex situ method. The thickness of the carbon shells should be considered as a key factor that can affect the performance of anodes. The optimized thickness of carbon layers can help to approach to the better performance of the anodes. However, the control of the carbon thickness is still a big challenge; more importantly, few reference was reported about the carbon thickness effect of core–shell structure on the battery performance.

* Corresponding author. Tel.: +1 519 6612111x87759; fax: +1 519 6613020.
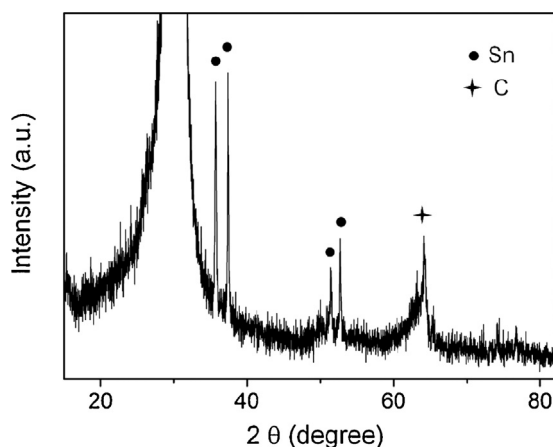E-mail address: xsun@eng.uwo.ca (X. Sun).

Fig. 1. XRD diffraction pattern of Sn@CNTs on carbon paper.

In this paper, we report an in situ method to synthesize encapsulated Sn nanowires in amorphous CNTs (Sn@CNTs), with tailored thickness of outer CNT shells. The thickness of outer CNT shells can be accurately controlled by using different experimental parameters: growth time, hydrocarbon gas flow rate and synthesis temperature. It was demonstrated that the carbon thickness has significantly affected cyclic performance of core–shelled anodes.

2. Experimental

2.1. Synthesis of Sn@CNTs

Sn@CNTs were synthesized by a CVD method [25]. Sn powder was used as the starting material and loaded in a ceramic boat which was placed in the center of a quartz tube. A piece of commercial carbon paper was used as the substrate and put near the Sn powder at the down stream of an Ar flow (400 sccm) which acted as carrier gas. The quartz tube was mounted in a tube furnace. Before the reaction started, the tube was purged by Ar flow for 15 min. When the furnace was heated up to the reaction temperature (800–900 °C), the nanostructures began to grow on the substrate under a mixed flow of Ar (400 sccm) and hydrocarbon gas (C_2H_4, 2–10 sccm). The system was kept at this condition for certain periods (0.5–2 h), and then was cooled down to the room temperature.

2.2. Materials characterization

The Sn@CNTs with different CNT shell thickness were characterized by X-ray diffraction (XRD, Rigaku Co Kα radiation), field emission scanning electron microscopy (FE-SEM, Hitachi 4800S SEM), transmission electron microscopy (TEM, Hitachi 7000), and high-resolution transmission electron microscopy (HRTEM, JEOL 2010 FEG).

2.3. Electrochemical measurement

The electrochemical measurements were carried out using coin-type half cells assembled in an argon-filled glove box. The Sn@CNTs growing on carbon papers were directly used as anodes after dried in a vacuum oven at 100 °C over night. A lithium foil worked as counter electrode. The electrolyte was prepared by dissolving 1 M $LiPF_6$ in a mixture of ethylene carbonate:diethyl carbonate:ethyl methyl carbonate with a volume ratio of 1:1:1. The charge/discharge cycling was performed galvanostatically in the range of 0.01–3.00 V at a constant current density of 100 mA g^{-1} [24,26]. Cyclic voltammetry (CV) curves were conducted in the range of 0.01–3.00 V at a scanning rate of 0.1 mV s^{-1}. The electrochemical measurements were conducted at room temperature.
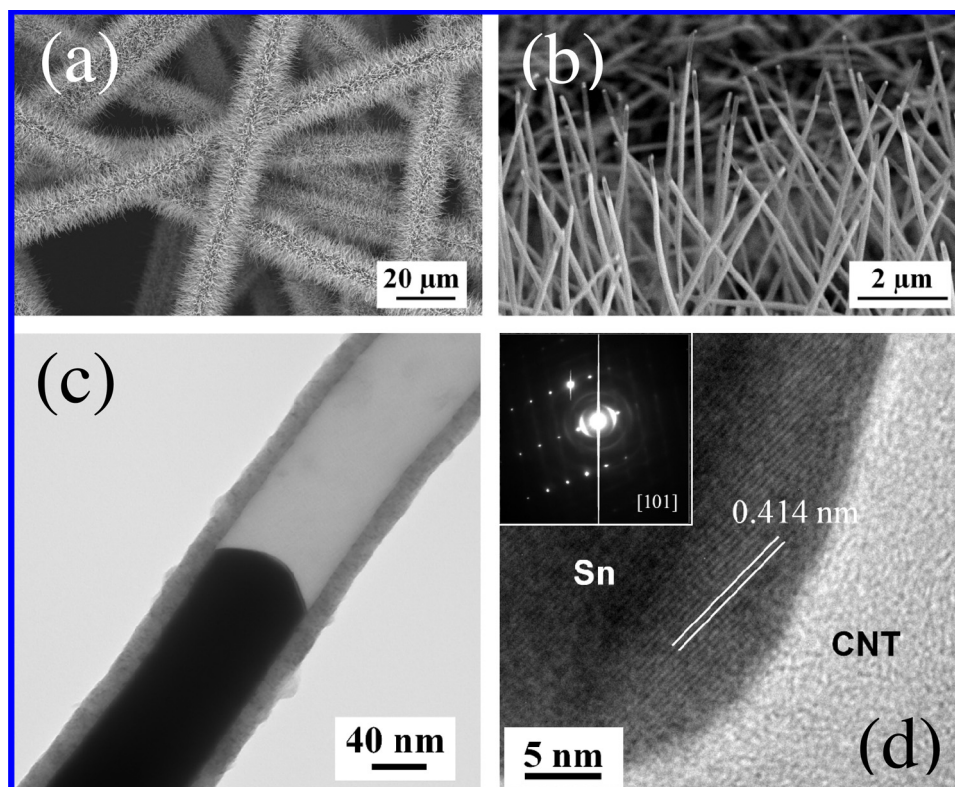

Fig. 2. SEM, TEM and HRTEM images of Sn@CNTs with amorphous CNT shell. (a) and (b) SEM images of Sn@CNTs; (c) and (d) TEM and HRTEM images, (d) inset: SAED of core.
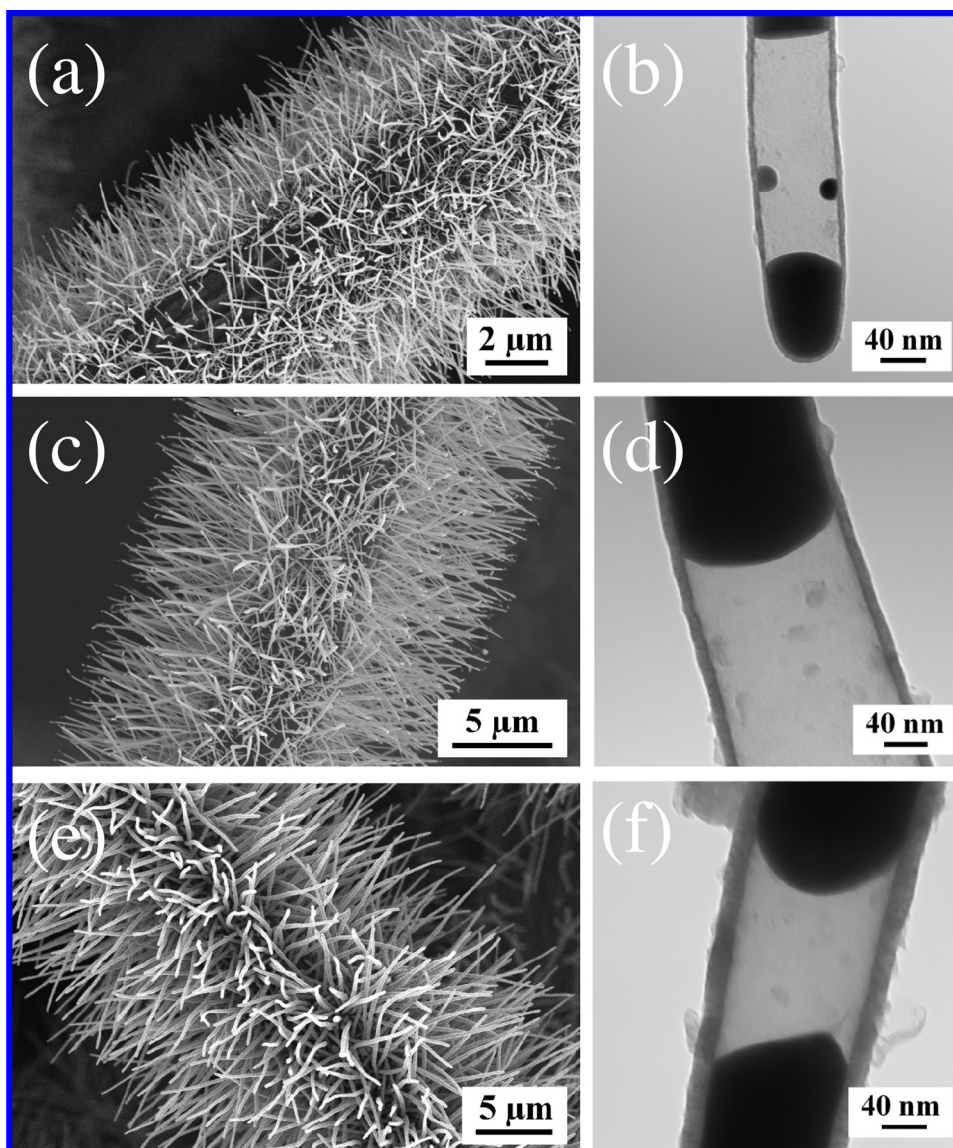
Fig. 3. SEM and TEM images of Sn@CNT with different growth time. (a) and (b) 0.5 h; (c) and (d) 1 h; (e) and (f) 2 h.

3. Results and discussion

Fig. 1 shows the XRD diffraction pattern of the as-synthesized products on the carbon paper substrate at 850 °C under C_2H_4 flow (5 sccm) for 2 h. The major peaks observed in the pattern are well indexed to tetragonal Sn (JCPDS card No. 04-0673). The peak assigned to graphite (JCPDS card No. 41-1487) is mainly derived from carbon substrate. The XRD pattern indicates the products present a relatively high purity.

Fig. 2a shows that the products are quite dense and completely cover the carbon substrate. The high resolution SEM image (Fig. 2b) reveals that the products exhibit the morphology of nanowires with the length ranging from 4 to 7 μm and average diameter around 170 nm. At the tips of the most nanowires, hollow cells are observed which are formed by very thin shell. Structural information was further investigated by TEM. Fig. 2c presents the TEM images of the products, which clearly reveals the products possess a core–shell structure. The core–shell structure consists of outer thin shell and inner solid core. The selected area electron diffraction (SAED) pattern of the solid core shown in Fig. 2d inset, is well indexed as β-Sn with the incident beam along [1 0 1] crystal

direction. The fringe spacing of the lattice of Sn nanowire was measured and labeled in Fig. 2d. The distance between two layers in the lattice is 0.414 nm which corresponds well to d spacing of {1 1 0} crystal planes of Sn with the standard crystal spacing of 0.412 nm [27,28]. On the other hand, the carbon shell in Fig. 2d presents the amorphous features. Clearly, the as-synthesized products have a core–shell structure consisting of crystalline Sn nanowires as core and amorphous carbon nanotubes as shell (Sn@CNTs). The growth mechanism of Sn@CNT involves the decomposition of C_2H_4, and absorption and diffusion of carbon precursors at Sn droplets acting as catalysts, followed by precipitation of CNT shell and growth of Sn nanowires [25]. Because of the low solubility of carbon, the catalytic ability of Sn is not effective, which leads to the growth of amorphous carbon in the materials [25]. The hollow cells were formed due to the shrinking derived from the conversion of Sn from liquid phase to solid phase during the cooling process.

The introduced outer CNT shells could effectively buffer the volume change during the charge/discharge process, and also helped to maintain the one dimensional nanostructure of the materials. However, the thickness of carbon shell has some influence on the 'buffering effect', and can affect the performance of the Sn@CNTs.
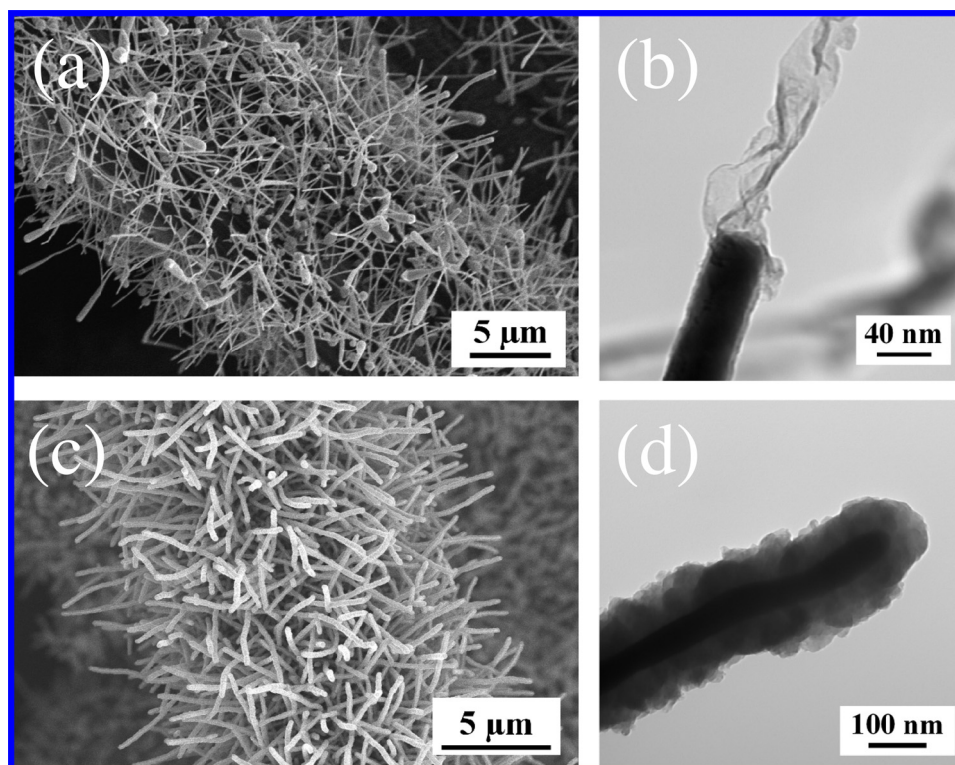
Fig. 4. SEM and TEM images of Sn@CNT with different carbon gas flow rates. (a) and (b) 2 sccm; (c) and (d) 10 sccm.

In order to control the thickness of the CNT shell, the effects of different experimental parameters on the carbon thickness were investigated, such as growth time, hydrocarbon gas flow rate and synthesis temperature.

To determine the effect of the growth time on the thickness of CNT shells, products were prepared in different growth time in 0.5, 1 and 2 h, respectively. After 0.5 h growth, a big amount of products with core–shell structure were observed (Fig. 3a). But there is still some area of carbon substrate exposed, which means the deposition time is not long enough to harvest the reaction species. The average length of Sn@CNTs is only around 3 μm. A very thin CNT shell forms outside the core with the average thickness of about 6 nm (Fig. 3b). As the growth time was prolonged to 1 h, dense Sn@CNTs were obtained with the average length of approximately 6 μm (Fig. 3c). The average thickness of CNT shell increased to 13 nm (Fig. 3d). When the growth time was continuously prolonged to 2 h, the Sn@CNTs became much denser and completely covered the carbon substrate (Fig. 3e). The average length increased to 10 μm. The outer CNT shell became quite thicker approximately to 18 nm (Fig. 3f). The above results illustrate that the thickness of CNT shell can be controlled by the growth time. At the initial growth stage, the content of the carbon species was low in the reaction zone. Increasing the growth time may enhance the supply of carbon precursors. Therefore, the growth of Sn@CNTs could be promoted. Then the longer growth time leads to the thicker CNT shell.

Hydrocarbon gas flow is another factor that can affect the growth of the outer CNT shell. To explore the effect, another two samples were produced at different C_2H_4 flow rates of 2 sccm and 10 sccm, respectively. As is known, the supply of carbon precursors is the key factor of the growth of Sn@CNTs [25]. At relatively small flow rate of C_2H_4 of 2 sccm, quite a few carbon precursors were released from the decomposition of C_2H_4. The supply of carbon precursors was not sufficient, which directly inhibited the growth of Sn@CNTs and resulted in low density of the products (Fig. 4a).

After reaction, the core–shell Sn@CNTs with the very thin CNT shell were obtained. The average thickness of the CNT shell is only 4 nm (Fig. 4b), much thinner than that prepared at the flow rate of 5 sccm. Due to the thin thickness and weak support, the carbon shell collapsed at the hollow part. In contrast, the big flow rate of C_2H_4 can enhance the growth of Sn@CNTs. At higher C_2H_4 flow rate of 10 sccm, both of the density of the products and the thickness of CNT shell increased (Fig. 4c and d). Especially, the CNT shell with the average thickness of 51 nm was obtained. The results demonstrate that the flow rate of C_2H_4 can greatly affect both the growth of Sn@CNTs and the thickness of the CNT shell. At higher flow rate of C_2H_4, more carbon precursors would be provided by decomposition of C_2H_4. These abundant carbon precursors activated the more growth sites and promoted the growth rate of CNT shell. Therefore, the enhanced the supply of carbon precursors could lead to the denser products and thicker CNT shell.

The effect of the temperature on the deposition of CNT shell was also investigated to approach an efficient route to control the thickness. Products were prepared at C_2H_4 flow rate of 5 sccm for 2 h growth time at 800 °C and 900 °C, respectively. At 800 °C, though the other experimental parameters were kept the same, the growth of nanostructures was apparently inhibited. After reaction, only a few Sn@CNTs were observed on the carbon substrate (Fig. 5a). Fig. 5b clearly reveals that the CNT shell in Sn@CNTs is very thin, with the average thickness of 4 nm, much thinner than that synthesized at 850 °C. When the temperature was increased to 900 °C, a large number of Sn@CNTs were found on the substrate (Fig. 5c). The biggest average thickness of CNT shell of 99 nm is achieved (Fig. 5d), much thicker than those synthesized at 800 °C and 850 °C. The decomposition rate of C_2H_4 was dominated by synthesis temperature. At higher temperature, the decomposition of C_2H_4 was promoted which could lead to the efficient supply of carbon precursors. Then the growth of Sn@CNTs was easily enhanced. Furthermore, more carbon precursors would join the growth of CNT shell, which could would great increase the thickness of CNT shell.
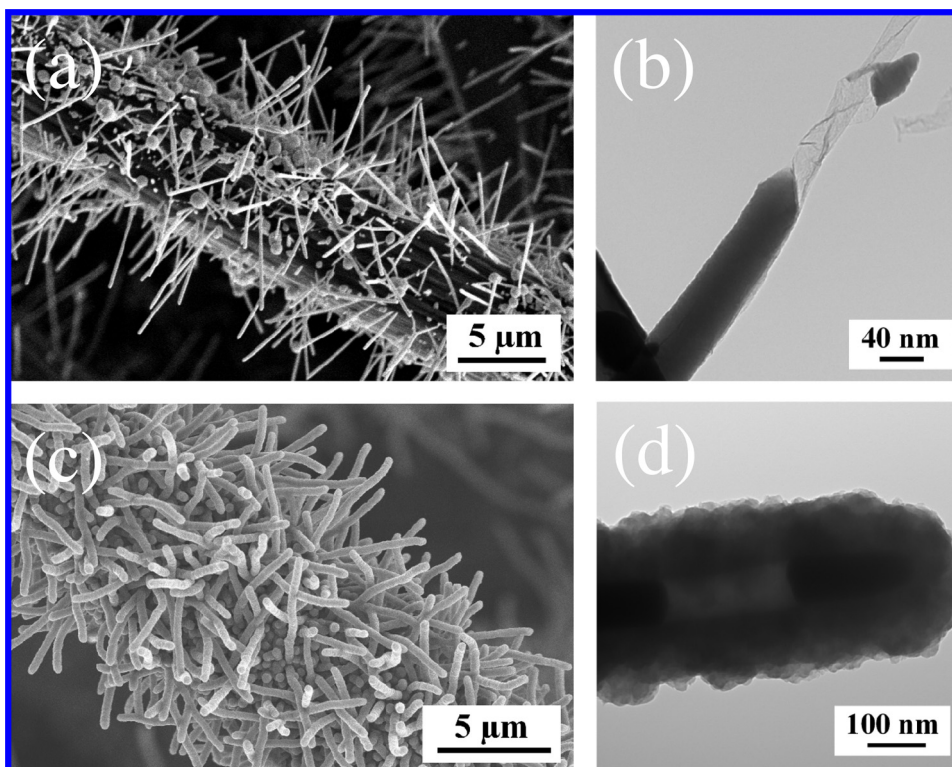
Fig. 5. SEM and TEM images of Sn@CNT with different temperatures. (a) and (b) Sn@CNT at 800 °C; (c) and (d) Sn@CNT at 900 °C.
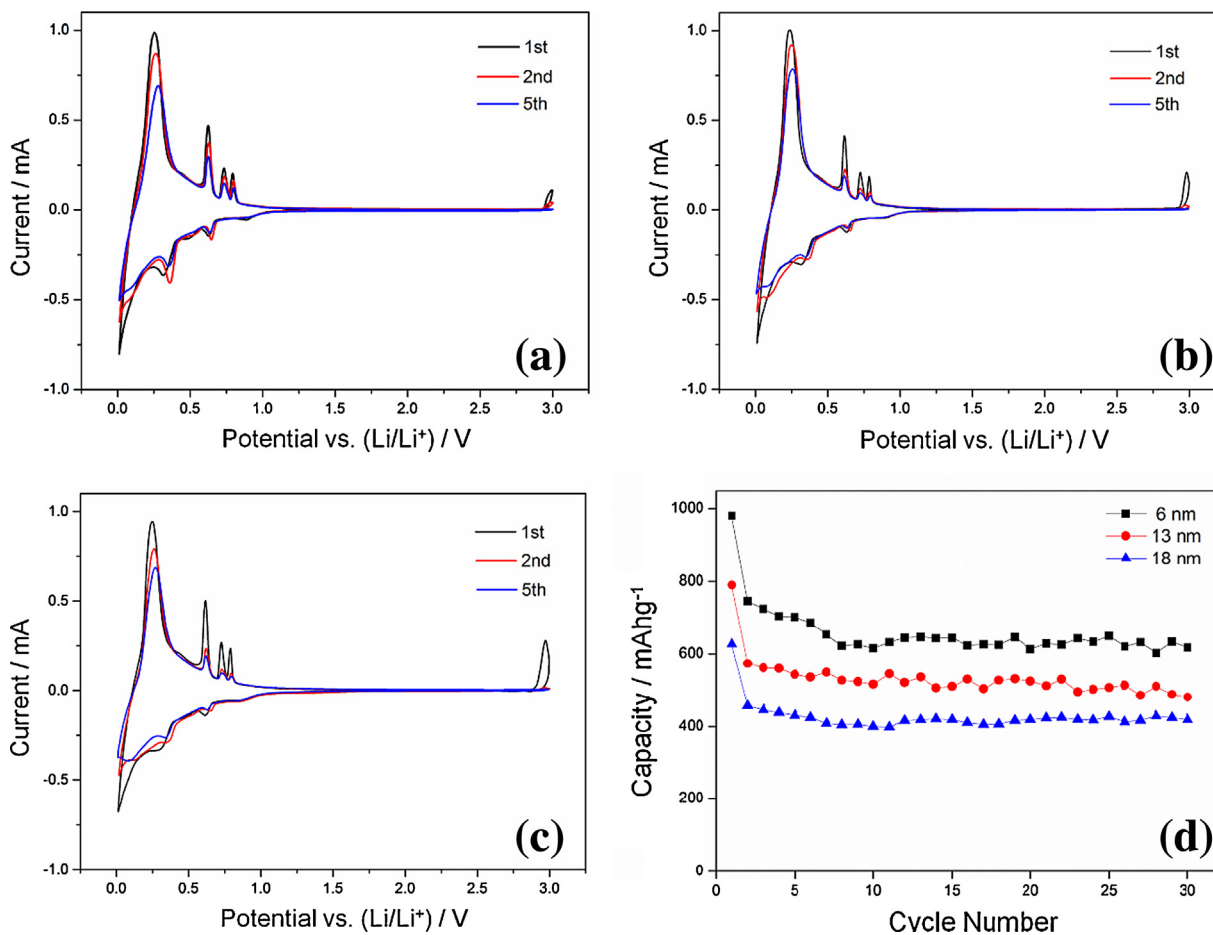

Fig. 6. The cycle voltammograms and cycle performance of Sn@CNTs with different CNT shell thickness. (a)–(c) The cycle voltammograms of Sn@CNT with CNT thickness of 6 nm, 13 nm and 18 nm; (d) the cycle performance of Sn@CNT with CNT thickness of 6 nm, 13 nm and 18 nm.

To evaluate the electrochemical behavior of Sn@CNTs with different thickness of CNT shells, the core–shell structures were investigated as anodes in half cells while the Li foils were used as the counter electrodes. Cyclic voltammograms (CVs) of Sn@CNTs with different CNT shell thickness are shown in Fig. 6a–c. There are three oxidation peaks observed at about 0.6, 0.7 and 0.8 V (vs. Li/Li$^+$) correspond to the extraction of Li$^+$ from Li$_x$Sn$_y$ alloys [29]; one oxidation peak at about 0.2 V (vs. Li/Li$^+$) is ascribed to the extraction of Li$^+$ from CNT shells [30]. Moreover, three reductions peaks appear at about 0.2, 0.4 and 0.6 V (vs. Li/Li$^+$), which are related to the insertion of Li$^+$ into Sn [29]. The reduction peak near 0.01 V (vs. Li/Li$^+$) is associated with the insertion of Li$^+$ into CNT shells [30]. The peak at round 0.85 V derived from the formation of SEI and should disappear after the first cycle. However, this peak was observed until the fifth cycle. This could be attributed to the formation of new surface deriving from the pulverization of electrode, at which the decomposition of the electrolyte and formation of SEI may continuously happen [31]. There is also one oxidation peak appearing at closed to 3.0 V in the first cycle, which could be attributed to the fresh surface of CNT shells [29]. As the thickness was increased, this peak became much bigger in thicker CNT shells.

The thickness of outer CNT shells can affect the performance of the Sn@CNTs. To demonstrate the effects, Sn@CNTs with different thickness of CNT shells (6 nm, 13 nm and 18 nm) were tested and the results of performance are displayed in Fig. 6d. The core–shell Sn@CNTs presented the exceptional capacity retention even with different thickness of CNT shells. The discharge capacity decayed after the first cycle, and then gradually stabilized. The main reason of the initial capacity loss is due to the irreversible formation of solid electrolyte interphase (SEI) [32]. The pulverization of the inner Sn nanowires derived from the volume expansion could also result in the capacity loss, but the outer CNT shells might buffer the volume expansion effectively and improve the performance [22]. Sn@CNTs with CNT shell of 6 nm in thickness presented the highest initial capacity of 980 mAh g^{-1}. The capacity sharply decreased after the first cycle due to the SEI formation and gradually stabilized around 630 mAh g^{-1} after 30 cycles. By compared materials with thin CNT shells, Sn@CNTs with the thicker CNT shells of 13 nm and 18 nm in thickness presented lower capacity around 520 mAh g^{-1} and 420 mAh g^{-1} after 30 cycles, respectively. Furthermore, the different thickness of CNT shells also influenced the retention of capacities. After 30 cycles, the Sn@CNTs with CNT shells of 18 nm in thickness remained 91.8% of reversible capacity of the second cycle, while the retention was 83.8% in Sn@CNTs with CNT shells of 13 nm, even further decreased to 83.0% in materials with much thinner CNT shells of 6 nm.

It is very clear that the outer CNT shells may help remain the structure and buffer the volume expansion. Moreover, the thickness of CNT shells can make an influence on the value and retention of the capacity. The thicker CNT shells can effectively maintain the structure during the working process, but the ratio of Sn which makes a major contribution to the capacity is reduced. Then the total capacity of the Sn@CNTs is low. On the other hand, as reducing the thickness of CNT shells, the ratio of Sn is promoted which can increase the total capacity of Sn@CNTs. However, due to the weak support, the thinner CNT shells could not effectively stabilized the structure, which might lead to fast fading of the capacity.

4. Conclusions

Sn@CNT core–shell structures were prepared by CVD method in one step. The thickness of outer CNT shells can be tailored by controlling the experimental conditions: growth time, flow rate of C$_2$H$_4$ and synthesis temperature. Sn@CNTs showed an excellent retention of capacity during the charge/discharge process. The cycle performance can be affected by the thickness of outer CNT shells. The thin CNT shells of 6 nm presented the highest capacity around 630 mAh g^{-1} after 30 cycles. Thicker CNT shells decreased the total capacity of Sn@CNTs, but presented a good retention of the capacity. The exceptional cycle performance is mainly attributed to the unique core–shell structure which effectively buffers the volume expansion and remains the structure of materials. The controlling the outer CNT shells provides an approach to design core–shell structures for Li ion battery application.

References

[1] P.G. Bruce, B. Scrosati, J.M. Tarascon, Angew. Chem. Int. Ed. 47 (2008) 2930.
[2] J.M. Tarascon, M. Armand, Nature 414 (2001) 359.
[3] M.G. Kim, J. Cho, Adv. Funct. Mater. 19 (2009) 1497.
[4] K. Kang, Y.S. Meng, J. Bréger, C.P. Grey, G. Ceder, Science 311 (2006) 977.
[5] S. PL Taberna, P. Mitra, P. Poizot, J.M. Simon, H. Tarascon, Nat. Mater. 5 (2006) 567.
[6] J. Hassoun, G. Derrien, S. Panero, B. Scrosati, Adv. Mater. 20 (2008) 3169.
[7] G. Derrien, J. Hassoun, S. Panero, B. Scrosati, Adv. Mater. 19 (2007) 2336.
[8] D. Larcher, S. Beattie, M. Morcrette, K. Edstroem, J.C. Jumas, J.M. Tarascon, J. Mater. Chem. 17 (2007) 3759.
[9] C.K. Chan, R.N. Patel, M.J. O'Connell, B.A. Korgel, Y. Cui, ACS Nano 4 (2010) 1443.
[10] L.Y. Beaulieu, K.W. Eberman, R.L. Turner, L.J. Krause, J.R. Dahn, Electrochem. Solid-State Lett. 4 (2001) A137.
[11] L. Fransson, E. Nordström, K. Edström, L. Häggström, J.T. Vaughey, M.M. Thackeray, Electrochem. Soc. Interface 149 (2002) A736.
[12] J.S. Chen, Y.L. Cheah, Y.T. Chen, N. Jayaprabash, S. Madhavi, Y.H. Yang, X.W. Lou, J. Phys. Chem. C 113 (2009) 20504.
[13] A.S. Aricò, P. Bruce, B. Scrosati, J.M. Tarascon, W.V. Schalkwijk, Nat. Mater. 4 (2005) 366.
[14] N. Li, C.R. Martin, B. Scrosati, Electrochem. Solid-State Lett. 3 (2000) 316.
[15] H. Mukaibo, A. Yoshizawa, T. Momma, T. Osaka, J. Power Sources 119–121 (2003) 60.
[16] W. Yin, B. Wei, C. Hu, Chem. Phys. Lett. 471 (2009) 11.
[17] A. Leonardy, W.Z. Hung, D.S. Tsai, C.C. Chou, Y.S. Huang, Cryst. Growth Des. 9 (2009) 3958.
[18] M.-R. Yang, S.Y. Chu, R.C. Chang, Sens. Actuators B 122 (2007) 269.
[19] M.S. Park, Y.M. Kang, G.X. Wang, S.X. Dou, H.K. Liu, Adv. Funct. Mater. 18 (2008) 455.
[20] L. Jankovič, D. Gournis, P.N. Trikalitis, I. Arfaoui, T. Cren, P. Rudolf, M.H. Sage, T.T.M. Palstra, B. Kooi, J.D. Hosson, M.A. Karakassides, K. Dimos, A. Moukarika, T. Bakas, Nano Lett. 6 (2006) 1131.
[21] X.W. Lou, C.M. Li, L.A. Archer, Adv. Mater. 21 (2009) 2536.
[22] W.M. Zhang, J.S. Hu, Y.G. Guo, S.F. Zheng, L.S. Zhong, W.G. Song, L.J. Wan, Adv. Mater. 20 (2008) 1160.
[23] N. Zhao, G. Wang, Y. Huang, B. Wang, B. Yao, Y. Wu, Chem. Mater. 20 (2008) 2612.
[24] X.W. Lou, D. Deng, J.Y. Lee, L.A. Archer, Chem. Mater. 20 (2008) 6562.
[25] R. Li, X. Sun, X. Zhou, M. Cai, X. Sun, J. Phys. Chem. C 111 (2007) 9130.
[26] D. Deng, J.Y. Lee, Angew. Chem. Int. Ed. 48 (2009) 1660.
[27] V.T. Deshpande, D.B. Sirdeshmukh, Acta Crystallogr. 14 (1961) 355.
[28] Y.J. Hsu, S.Y. Lu, J. Phys. Chem. B 109 (2005) 4398.
[29] S. Liang, X. Zhu, P. Lian, W. Yang, H. Wang, J. Solid State Chem. 184 (2011) 1400.
[30] G. Wang, Y.Q. Ma, Z.Y. Liu, J.N. Wu, Electrochim. Acta 65 (2012) 275.
[31] M. Park, G. Wang, Y. Kang, D. Wexler, S. Dou, H. Liu, Angew. Chem. Int. Ed. 46 (2007) 750.
[32] Y.S. Jung, K.T. Lee, J.H. Ryu, D. Im, S.M. Oh, J. Electrochem. Soc. 152 (2005) A1452.